

# Electron-channel blockade for plasmonic wavepackets

Shintaro Takada,<sup>1,2,3,4,\*</sup> Giorgos Georgiou,<sup>5</sup> Junliang Wang,<sup>6</sup> Yuma Okazaki,<sup>1</sup>  
Shuji Nakamura,<sup>1</sup> David Pomaranski,<sup>7</sup> Arne Ludwig,<sup>8</sup> Andreas D. Wieck,<sup>8</sup>  
Michihisa Yamamoto,<sup>7,9</sup> Christopher Bäuerle,<sup>6</sup> and Nobu-Hisa Kaneko<sup>1</sup>

<sup>1</sup>*National Institute of Advanced Industrial Science and Technology (AIST),*

*National Metrology Institute of Japan (NMIJ), 1-1-1 Umezono, Tsukuba, Ibaraki 305-8563, Japan*

<sup>2</sup>*Department of Physics, Graduate School of Science, Osaka University, Toyonaka, 560-0043, Japan*

<sup>3</sup>*Institute for Open and Transdisciplinary Research Initiatives, Osaka University, Suita, 560-8531, Japan*

<sup>4</sup>*Center for Quantum Information and Quantum Biology (QIQB), Osaka University, Osaka 565-0871, Japan*

<sup>5</sup>*James Watt School of Engineering, Electronics and Nanoscale Engineering,  
University of Glasgow, Glasgow, G12 8QQ, U.K.*

<sup>6</sup>*Université Grenoble Alpes, CNRS, Grenoble INP, Institut Néel, F-38000 Grenoble, France*

<sup>7</sup>*Department of Applied Physics, University of Tokyo, Bunkyo-ku, Tokyo, 113-8656, Japan*

<sup>8</sup>*Lehrstuhl für Angewandte Festkörperphysik, Ruhr-Universität Bochum,  
Universitätsstraße 150, D-44780 Bochum, Germany*

<sup>9</sup>*Center for Emergent Matter Science, RIKEN, Wako, Saitama, 351-0198, Japan*

(Dated: March 11, 2025)

Collective excitation of an interacting electron liquid called plasmon has distinct properties compared to those of a bare electron. Plasmons excited by a short voltage pulse and transmitted through quantum devices will distribute amongst electron conduction channels via Coulomb interactions, which is known as charge fractionalization. This process spreads plasmons into all Coulomb-coupled electron conduction channels, including those in neighbouring circuits, and makes it difficult to control them in quantum circuits. Here we demonstrate the isolation and on-demand selection of electron conduction channels contributing to the plasmon using a cavity, which enables us to control the velocity of propagating plasmons. We demonstrate an electron-channel blockade effect, where charge fractionalization to cavity-confined electron conduction channels is prohibited by the narrow energy distribution of the plasmon itself. This effect is unaffected by the energy fluctuation of the surrounding circuits. The electron-channel blockade offers a powerful tool for designing plasmonic circuits as it can be used to control the plasmon velocity by local parameters, suppress unwanted plasmonic excitation in nearby circuits, and select electron-channels of plasmon eigenstates in quantum interferometers.

The interaction of free electrons with electromagnetic waves has been long known to induce plasmons. This collective motion of a free electron gas is the reason that metals have their characteristic colours and what makes them perfect mirrors. Ever since the early 2000s, plasmons have been used for studying strong light-matter interactions, also known as surface plasmon polaritons [1, 2]. Due to their sub-wavelength confinement they have enabled spectroscopy sensing at a molecular level and the development of perfect lenses [3] and metasurfaces [4].

In two-dimensional electron gases (2DEGs), plasmons present at microwave and far infrared frequencies due to the relatively low electron concentration in the 2DEGs [5, 6]. Because of their large momentum mismatch with photons, 2D plasmons were traditionally excited by in-plane gratings to add extra momentum to free-space photons. It was recently demonstrated, however, in semiconductors and graphene systems that 2D plasmons can be excited in heterostructures using picosecond voltage pulses [7, 8].

Overcoming the limitations of 2D plasmon excitation

in heterostructures has set strong foundations for plasmon quantum circuits. This has been further stimulated by the advancement of single electron sources based on Lorentzian pulses [9] that have been used to create plasmonic excitations in 2D materials carrying the equivalent of a single electron without creating holes in the Fermi sea [10–12]. It was recently proposed that plasmon excitations can be used as the carrier of quantum information in electron quantum optics systems [13–16]. In analogy to quantum optics, quantum information can be encoded on a flying electron, which can be controlled in-flight as it propagates through well defined electronic waveguides [17–19]. Their potential use for quantum information and sensing applications has been further reinforced by their robust coherent properties [20, 21].

In a quantum circuit composed of quasi-one-dimensional quantum wires, an eigenstate of a plasmon wavepacket can be described as a charge mode of a Tomonaga-Luttinger liquid (TLL) [22]. The plasmon eigenstate in these systems is formed by all the electron conduction channels below the Fermi energy, which are coupled together via Coulomb interactions. These interactions can result into non-trivial propagation of plasmons and can cause charge fractionalization [23, 24] and spin-charge separation [25–27], as shown in quantum Hall systems with one or two conduction channels [28–30]. At

---

\* corresponding authors: takada@phys.sci.osaka-u.ac.jp

zero magnetic fields, controlling the plasmon eigenstates and thus their propagation properties can be achieved by electrostatic Schottky gates [7]. By using the gates defining the quantum wire, one can control the number of available conduction channels, and thus modify on-demand the plasmon wavepacket speed. In an ideal circuit, a plasmon propagating through a single conduction channel will have almost the same speed throughout the device and quantum information carried by the plasmon will be controlled by the interference of the channel. However, realising single conduction channels at zero magnetic fields is challenging due to nanofabrication imperfections and impurities because of reduced charge screening effects. Controlling the eigenstate of plasmons in large quantum circuits through electrostatic gates, can release some of the nanofabrication constraints, enabling complex circuits with multiple components and at zero magnetic fields.

In this article, we reveal a novel phenomenon which we call *electron-channel blockade* for plasmon wavepackets, that can effectively suppress additional electron conduction channels in a quasi-1D wire, therefore allowing plasmon propagation into a single channel. This can be realized by forming a cavity between two local constrictions embedded in a long quantum wire. The electron-channel blockade can be triggered by an external voltage on the local gate and can be used to control on demand the eigenstate of plasmon wavepackets. Since the eigenstate is directly related to the speed of the plasmon wavepacket, it is used to control the speed and hence can be applied for a delay line in plasmonic quantum circuits. Furthermore, the electron-channel blockade allows us to suppress excitation of plasmons in circuits including those in nearby circuits.

## I. TIME-RESOLVED MEASUREMENT OF PLASMON WAVEPACKETS

Our quantum device consists of a 100  $\mu\text{m}$ -long electron waveguide, fabricated by depositing electrostatic gate electrodes on a GaAs/AlGaAs heterostructure, as schematically drawn in Fig. 1a. The waveguide length can be adjusted using two segments, labelled w1 and w2. By applying a negative gate voltage to these surface gates, the underlying two-dimensional electron gas (2DEG) can be depleted, allowing for the formation of either a 50  $\mu\text{m}$  waveguide (w2) or a 100  $\mu\text{m}$  waveguide when both segments (w1 + w2) are combined. Electrons are injected into the 2DEG by applying a voltage pulse  $V_{\text{in}}(t)$ , with variable duration, to the left Ohmic contact  $O_i$ , using an Arbitrary Waveform Generator (AWG, Keysight M8195A). They propagate in the form of a plasmon wavepacket through the quantum device. For detection, we utilize the right Ohmic contact,  $O_o$ , where the current is converted into voltage across a 10 k $\Omega$  resistor, then amplified and measured. The quantum point contacts (QPCs) at the entrances of the two waveguides,

highlighted in red and blue, are used to locally control the number of transmitting electron conduction channels, while the QPC at the waveguide exit, highlighted in purple, is used to measure the speed of plasmon wavepackets via time-resolved measurements following reference [7]. Fig. 1b illustrates the shape of the voltage pulses used in the measurement of this device. For our measurements, we applied voltage pulses with temporal widths varying from 52 ps to 500 ps. The displayed pulse shapes were recorded at the output of the AWG using a sampling oscilloscope at room temperature.

Time-resolved measurements are performed using QPC3, that plays the role of an ultrafast on/off switch thus enabling in-situ stroboscopic probing. Initially, QPC3 is closed by applying a sufficiently large negative gate voltage to the DC port of the bias-tee, ensuring zero conductance across the waveguide. To probe the propagating wavepacket, QPC3 is briefly switched “on” by applying a 52 ps-long positive voltage pulse,  $V_{\text{det}}(t)$ , to the upper gate of QPC3 through the RF port of the bias-tee. This pulse allows a small fraction of the plasmon wavepacket to pass through QPC3. By varying the time delay between the generation of the plasmon wavepacket triggered by a voltage pulse  $V_{\text{in}}(t)$  and the detection pulse  $V_{\text{det}}(t)$  at QPC3, we can reconstruct the temporal profile of the wavepacket in a time-resolved manner. To obtain an absolute value for the plasmon propagation speed, we carefully calibrate the length difference of the RF lines, using the known propagation speed of the two-dimensional plasmon (see Methods). To obtain a measurable current we repeat the procedure at a repetition rate of 250 MHz. In addition we modulate the injected pulse on  $O_i$  at 12 kHz and measure the output current at  $O_o$  with lock-in technique to enhance the signal-to-noise ratio. The measured current at  $O_o$ , represents, in principle, the convolution of the plasmon wavepacket propagating through the electron waveguide with the time-dependent conductance across QPC3. The speed of the plasmon wavepacket,  $v_p$ , is then calculated from the peak delay,  $t_p$ , and the length of the quantum wire,  $L_{\text{wire}}$ , using the relation  $v_p = L_{\text{wire}}/t_p$ . As a control experiment, we perform time-resolved measurements of the plasmon wavepacket generated by a 180 ps-long voltage pulse in the 50  $\mu\text{m}$ -long electron waveguide, varying the side gate voltage  $V_{w2}$ . This reduces the number of available electron conduction channels inside the waveguide, leading to a slowing down of the propagation, as demonstrated in reference [7]. Our experimental results (Figs. 1c, d) reproduce this behaviour, and the obtained propagation speeds are consistent with the previous study [7]. In the following measurements, we employ  $V_{\text{in}}$  with different temporal widths having the similar peak amplitude. The peak amplitude is slightly varied due to the bandwidth of the AWG from 1.9 mV for the shortest (52 ps-long) voltage pulse to 2.6 mV for the longest (500 ps-long) voltage pulse. We carefully verified that for a given pulse width the plasmon speed, or equivalently the peak position, is independent with respect to the peak amplitude.

In Fig. 1e, we present representative data for a voltage pulse with a temporal width of 180 ps, demonstrating that the peak position remains constant regardless of the voltage pulse's peak amplitude

## II. LOCAL CONTROL OF TRANSMITTING ELECTRON CHANNELS

We now perform time-resolved measurements, while controlling the number of transmitting electron conduction channels at QPC1 in the 100  $\mu\text{m}$ -long electron waveguide. The voltage applied to the gates w1, w2 is set so that the waveguide accommodates more than 20 conduction channels. Fig. 2a shows the results obtained with 52 ps-long voltage pulse. The pulse peak position,  $t_p$ , stays fixed at 100 ps and does not shift when the number of the transmitting conduction channels through QPC1 is modified. In addition, the detected peak shape has a longer tail at larger time delays, showing additional peaks. In particular the second peak appears around 220 ps, which is less than  $3 \cdot t_p$  and hence it does not originate from the wavepacket reflected back and forth between QPC1 and QPC3. This result indicates that the plasmon wavepacket is being redistributed to the eigenstates formed by all the conduction channels in the waveguide after passing through QPC1 locally limiting the number of the transmitting conduction channels. This process is known as charge fractionalization [29]. Our result shows the microscopic dynamics of this process.

On the other hand, when we perform the same measurement with 500 ps-long voltage pulses, a completely different result is obtained, as shown in Fig. 2b. Here the peak position,  $t_p$  shifts to a larger delay when the number of the transmitting conduction channels is locally reduced at QPC1. The speed of the plasmon wavepackets as a function of  $V_{\text{QPC1}}$  calculated from the data in Figs. 2a, b is summarised in Fig. 2c. For the shorter pulse the speed is constant as a function of  $V_{\text{QPC1}}$ . This is caused by the redistribution of the wavepacket into the eigenstates of the waveguide right after QPC1. For the longer pulse the speed is controlled by  $V_{\text{QPC1}}$  and hence by the number of the local transmitting conduction channels. This result implies that the charge fractionalization process is suppressed for a longer plasmon wavepacket. Further to that, we note that the speed of the plasmon wavepackets generally decreases for those excited by longer pulses and should approach the Fermi velocity in the DC limit (see Fig. S4 in details).

## III. FABRY-PÉROT CAVITY AND ELECTRON-CHANNEL BLOCKADE

To interpret the behaviour observed in Fig. 2 we focus on the Fabry-Pérot (FP) cavity, which is formed between QPC1 at the entrance, and QPC3 at the exit

of the electron waveguide. For the time-resolved measurement, QPC3 is pinched off and is opened only for a short time, therefore forming one of the two end mirrors of the FP cavity. The second one, is a partially transmitting end mirror to this FP cavity, formed by QPC1. As the FP cavity can be set to contain many conduction channels, when QPC1 is narrowed, electron conduction can only take place through a small number of transmitting channels. The channels which cannot transmit through the QPC are fully confined inside the FP cavity. The quantised energy levels of the FP cavity is the origin of the electron-channel blockade, as it allows for selecting the conduction channels contributing to the wavepacket transmission, when the matching conditions are met. Let us suppose that the electron waveguide contains  $N$  conduction channels and QPC1 is tuned to transmit exactly 1 conduction channel. In this case,  $(N - 1)$  conduction channels are confined inside the cavity. The resonant cavity condition is given by  $\lambda_m = 2L_{\text{FP}}/m$ , where  $m$  is a positive integer corresponding to the mode number of the FP cavity. Similarly, the frequency components of the wavepacket which is transmitted through QPC1 should satisfy the resonant condition,  $f_m = m \cdot v_p / (2L_{\text{FP}}) = m \cdot \Delta f$ , where  $v_p$  is the speed of the plasmon wavepacket. On the other hand, the generated plasmon wavepacket is composed of many frequency harmonics and its excitation spectrum contains frequency components up to the cut-off frequency,  $f_c \sim 1/t_{\text{FWHM}}$  (see Figs. 3b, c).

When  $f_c$  is smaller than  $\Delta f$ , the frequency components necessary to construct a plasmon standing wave within the cavity are not available, and the  $(N - 1)$  confined channels cannot contribute to the plasmon wavepacket transmission. As a result, charge fractionalization to the  $(N - 1)$  conduction channels is blocked. The plasmon is funnelled and transmitted only through the eigenstate of a *single* electron conduction channel. We call this phenomenon as *electron-channel blockade* for plasmon wavepackets. In the opposite limit  $f_c \gg \Delta f$ , the Fabry-Pérot resonance condition is fulfilled and as a result, a plasmon standing wave can be formed inside the FP cavity. For a non-interacting system, the plasmon can form a standing wave with a single conduction channel. A plasmon, however, is a collective excitation of interacting electrons. As it travels within the cavity, charge fractionalization occurs and it will populate the eigenstates of the remaining  $N - 1$  conduction channels. In this situation the speed of plasmons cannot be controlled with the channel selection QPC, as the velocities within the cavity will be renormalised due to Coulomb interactions and a  $N$ -channel plasmon mode appears as a main component (for a detailed theory see the Supplementary Information in [7]).

Figure 3a shows  $\Delta f/f_c$  calculated from the data in Fig. 2c for the plasmon wavepackets excited by a 52 ps and 500 ps-long voltage pulse. For the longer pulse  $\Delta f$  exceeds  $f_c$  for all  $V_{\text{QPC1}}$  values and hence electron-channel blockade occurs, enabling plasmon speed control

with QPC1. Conversely, for the shorter pulse,  $\Delta f$  is a few times smaller than  $f_c$ . In this case, the plasmon speed remains constant with respect to  $V_{\text{QPC1}}$ . Those observations are in line with our hypothesis discussed above. For  $\Delta f > f_c$ , which translates to  $L_p = v_p \cdot t_{\text{FWHM}} > 2L_{\text{FP}}$ , plasmon transport through the electron conduction channels confined inside the FP cavity is blocked and hence we can control the plasmon speed by locally changing the number of the transmitting conduction channels at QPCs. For  $L_p \ll 2L_{\text{FP}}$  charge fractionalization occurs within the cavity and hence the plasmon eigenstate cannot be controlled by QPCs.

To confirm our hypothesis we intentionally break the FP cavity and demonstrate that, in this case, the QPC at the entrance of the waveguide is no longer effective to control the plasmon speed or its eigenstate. To do this, we completely depolarize the middle gate of  $g_{\text{res}}$ , highlighted in green in Fig. 1a, to open the FP cavity towards the Ohmic contact  $O_r$ . This connection to the Fermi sea reservoir breaks the FP cavity. We then perform time-resolved measurements as a function of  $V_{\text{QPC1}}$ , for the 500 ps-long pulse, and compare the result with the configuration where the FP cavity is not broken (see Figs. 3d, e). When comparing the plasmon speed as a function of  $V_{\text{QPC1}}$ , we observe that the plasmon travels significantly faster and shows smaller variation with  $V_{\text{QPC1}}$ . In principle, we expect the plasmon speed to be entirely independent of  $V_{\text{QPC1}}$ . However, this is not observed, as the opening to the reservoir accounts for less than 1% of the total length of the FP cavity. As a result, the quality factor of the cavity is reduced but the FP cavity is still influencing the plasmon speed. To further validate our observations, we confirm that in a three-terminal device (a quantum wire with two outputs), the local selection of the number of transmitting electron channels with a QPC does not affect the speed of plasmon wavepackets, as no FP cavity is involved (see Fig. S6.)

The demonstrated electron channel blockade using a FP cavity originates from the narrower energy spectrum of plasmon wavepackets compared to the energy quantisation of the FP cavity. This mechanism is not affected by the energy fluctuation of the reservoirs at higher temperatures. Indeed, when we perform the same measurement as Fig. 2 at 4 K in a slightly different gate voltage configuration, we find the same tendency (see Fig. S5). Here the energy fluctuation of the reservoir is much larger than  $\Delta f$  of the FP cavity. This is in clear contrast to Coulomb blockade of electron transport through a quantum dot, where the blockade is lifted at larger energy fluctuations of the reservoirs than the quantised energy of the quantum dot at high temperatures.

#### IV. SUPPRESSION OF CHARGE FRACTIONALIZATION IN PARALLEL WAVEGUIDES

The conduction of electrons in two parallel, yet electrically isolated, electron waveguides can be considered independent. However, even though direct exchange of electrons is prohibited between the two parallel waveguides, electrons are coupled through Coulomb interactions. As a result, when a plasmon wavepacket is injected into one path of the two waveguides, charge fractionalization occurs and a plasmon wavepacket is induced at the other waveguide [28].

Here we demonstrate the suppression of the charge fractionalization in such a parallel waveguides using the electron channel blockade demonstrated above. For this measurement we use a device shown in Fig. 4a (see Method for details of the device). We form the two parallel electron waveguides by depleting the gates coloured in yellow. The two waveguides are electrically isolated by the middle gate along the waveguides and the upper gate at the entrance on the left highlighted in purple. Plasmon wavepackets are injected by applying a 83 ps-long voltage pulse from an AWG (Keysight M8190A) on the left-most Ohmic contact,  $O_{\text{inj}}$ , with the peak amplitude of  $\sim 1.6$  mV. They propagate through the lower electron waveguide and are collected in  $O_1$ . Here, plasmon wavepackets are expected to be induced at the upper electron waveguide [28]. To measure these induced wavepackets, we perform a time-resolved measurement using QPC<sub>det</sub> at the upper waveguide. For consistency, the probe pulse at QPC<sub>det</sub>, is also 83 ps-long. In this device we can form a FP cavity at the upper electron waveguide by using the gate,  $g_{\text{FP}}$ , marked in red colour. When the FP cavity is not formed, the induced plasmon wavepacket is observed as expected (the blue curve in Fig. 4b). The shape of the induced wavepacket is similar to the derivative of the injected wavepacket whose shape is characterised in a slightly different setup from Fig. 4a (see Fig. S7 in details). The derivative-like shape can be understood as a current induced by the capacitive coupling with the charge of the injected wavepacket. On the other hand, by applying a large negative voltage on  $g_{\text{FP}}$  to deplete the 2DEG underneath and by forming the FP cavity there is no Coulomb-induced plasmon wavepacket as shown by the orange curve in Fig. 4b. When we estimate  $L_p$  and  $2L$  in this situation, they are about 33  $\mu\text{m}$  and 40  $\mu\text{m}$ , respectively. While this does not strictly satisfy the condition for electron-channel blockade ( $L_p > 2L$ ), the observed suppression of induced charge at  $L_p \sim 2L$  strongly suggests its effectiveness. Given the limitations in precisely quantifying this condition, we attribute this suppression to electron-channel blockade within the FP cavity formed on the upper quantum wire.

## V. CONCLUSIONS

We have investigated the propagation of ultrashort plasmon wavepackets in a quantum nanoelectronic circuit while controlling the number of transmitting electron conduction channels at local constrictions. We found that a FP cavity formed by two potential barriers plays a critical role for the propagation of plasmon wavepackets. When the spatial length of the plasmon wavepacket,  $L_p(\equiv v_p \cdot t_{FWHM})$ , is longer than double the length of the FP cavity, electron-channel blockade occurs, where plasmon eigenstate or speed can be controlled by changing the number of the transmitting conduction channels at local constrictions. Controlling the speed of ultrashort plasmonic excitations is attractive for quantum applications and the field of electron quantum optics. In particular, modifying the speed is equivalent to a phase delay and can be used for controlling the quantum state of a plasmon flying qubit [12, 20, 31]. With this method a long one-dimensional system can be realised by placing a QPC at a distance  $L$  shorter than  $L_p/2$  as shown in Fig. 5 and setting all the QPCs to allow transmission of only a single electron conduction channel. Since most of the electron waveguide can be kept wide, the stronger screening due to higher electron density makes plasmon wavepackets less vulnerable to potential fluctuations in the surrounding environment. Furthermore, electron-channel blockade can be used to suppress unwilling leakage of plasmon wavepackets to nearby circuits. This will contribute to high-fidelity operations of a plasmon quantum state. We expect that the demonstrated electron-channel blockade will empower precise control of plasmon wavepackets in quasi-1D electron waveguides, significantly advancing the development of both quantum and high-frequency classical circuits based on plasmons.

## METHODS

**Device fabrication** The device was fabricated in a GaAs/AlGaAs heterostructure hosting a 2DEG at 110 nm (140 nm for the device in Fig. 4, Figs. S6 and S7) below the surface. The electron density and the mobility of the 2DEG are  $2.8 \times 10^{11} \text{ cm}^{-2}$  and  $9.0 \times 10^5 \text{ cm}^2 \text{ V}^{-1} \text{ s}^{-1}$  ( $2.1 \times 10^{11} \text{ cm}^{-2}$  and  $1.9 \times 10^6 \text{ cm}^2 \text{ V}^{-1} \text{ s}^{-1}$  for the device in Fig. 4, Figs. S6 and S7) at 4 K, respectively. The Schottky gates to define the quantum wires and the QPCs were defined by Ti/Au and the Ohmic contacts were defined by Ni/Ge/Au/Ni/Au alloy. A scanning electron microscope image of the device in Figs. 1-3 is shown in Fig. S1. All measurements except for the ones in Figs. 1b, e were performed at the base temperature of a dilution refrigerator around 15 mK. Characterisation measurement in Fig. 1b was performed at room temperature and the one in Fig. 1e was performed at 4 K.

**Calibration of RF lines** The time delay between the pulses travelling through the RF injection and the

detection lines is influenced by the attenuators placed on each line. The delay is fixed for each RF line and can be the order of ps. To accurately evaluate the speed of plasmon wavepackets this time delay should be properly calibrated. For this, we used a two dimensional (2D) plasmon excitation, as in Ref. [7], since a 2D plasmon is known to be as fast as  $1.0 \times 10^7 \text{ m/s}$  [32, 33]. When we set the voltage of the gates forming the quantum wire to zero, the excited plasmon wavepackets propagate through the device as 2D plasmon excitation, which is detected at QPC3. The time-resolved measurement of the 2D plasmons excited by the voltage pulses with different temporal lengths are plotted in Fig. S2. From the time delay at the peak of each curve we obtain the relative time delay between the two RF lines as 111(6) ps. We use this as a zero time delay for the plasmon wavepacket time-resolved measurements with an error bar of 6 ps. The same calibration is performed for the device in Fig. 4.

## DATA AVAILABILITY

Relevant data supporting the key findings of this study are available within the article and the Supplementary figures. All raw data generated during the current study are available from the corresponding author upon request.

## ACKNOWLEDGMENTS

S.T., M.Y. acknowledges financial support from JST Moonshot R & D grant no. JPMJMS226B. This work was supported by a joint JST-ANR Research Project through Japan Science and Technology Agency, CREST (grant number JPMJCR1876) and the French Agence Nationale de la Recherche, Project QCONTROL ANR-18-JSTQ-0001 and has been done in the framework of the International Research Project ‘‘IRP FLEQ’’ between CNRS, RIKEN, AIST and Osaka University. This project has received funding from the European Union H2020 research and innovation program under grant agreement No. 862683, ‘‘UltraFastNano’’. GG acknowledges financial support from EPSRC QUANTERAN (EP/X013456/1), Royal Society of Edinburgh projects TEQNO and TFLYQ. C.B. acknowledges funding from the Agence Nationale de la Recherche under the France 2030 programme, reference ANR-22-PETQ-0012. J.W. acknowledges the European Union H2020 research and innovation program under the Marie Skłodowska-Curie grant agreement No. 754303. Views and opinions expressed are those of the author(s) only and do not necessarily reflect those of the European Union or the granting authority. Neither the European Union nor the granting authority can be held responsible for them.

- 
- [1] T. W. Ebbesen, H. J. Lezec, H. F. Ghaemi, T. Thio, and P. A. Wolff, Extraordinary optical transmission through sub-wavelength hole arrays, *Nature* **391**, 667 (1998).
- [2] S. A. Maier, *Plasmonics: Fundamentals and Applications* (2007).
- [3] J. B. Pendry, Negative refraction makes a perfect lens, *Phys. Rev. Lett.* **85**, 3966 (2000).
- [4] N. Yu, P. Genevet, M. A. Kats, F. Aieta, J. P. Tetienne, F. Capasso, and Z. Gaburro, Light propagation with phase discontinuities: generalized laws of reflection and refraction, *Science* **334**, 333 (2011).
- [5] S. J. Allen, D. C. Tsui, and R. A. Logan, Observation of the two-dimensional plasmon in silicon inversion layers, *Phys. Rev. Lett.* **38**, 980 (1977).
- [6] R. J. Wilkinson, C. D. Ager, T. Duffield, H. P. Hughes, D. G. Hasko, H. Ahmed, J. E. F. Frost, D. C. Peacock, D. A. Ritchie, G. A. C. Jones, C. R. Whitehouse, and N. Apsley, Plasmon excitation and self-coupling in a bi-periodically modulated two-dimensional electron gas, *Journal of Applied Physics* **71**, 6049 (1992).
- [7] G. Roussely, E. Arrighi, G. Georgiou, S. Takada, M. Schalk, M. Urdampilleta, A. Ludwig, A. D. Wieck, P. Armagnat, T. Kloss, X. Waintal, T. Meunier, and C. Bäuerle, Unveiling the bosonic nature of an ultrashort few-electron pulse, *Nature Communications* **9**, 2811 (2018).
- [8] K. Yoshioka, G. Bernard, T. Wakamura, M. Hashisaka, K.-i. Sasaki, S. Sasaki, K. Watanabe, T. Taniguchi, and N. Kumada, On-chip transfer of ultrashort graphene plasmon wave packets using terahertz electronics, *Nature Electronics* **7**, 537 (2024).
- [9] J. Dubois, T. Jullien, F. Portier, P. Roche, A. Cavanna, Y. Jin, W. Wegscheider, P. Roulleau, and D. C. Glattli, Minimal-excitation states for electron quantum optics using levitons, *Nature* **502**, 659 (2013).
- [10] R. Bisognin, A. Marguerite, B. Roussel, M. Kumar, C. Cabart, C. Chapdelaine, A. Mohammad-Djafari, J. M. Berroir, E. Bocquillon, B. Placais, A. Cavanna, U. Gennser, Y. Jin, P. Degiovanni, and G. Fève, Quantum tomography of electrical currents, *Nature Communications* **10**, 3379 (2019).
- [11] M. Aluffi, T. Vasselon, S. Ouacel, H. Edlbauer, C. Geffroy, P. Roulleau, D. C. Glattli, G. Georgiou, and C. Bäuerle, Ultrashort electron wave packets via frequency-comb synthesis, *Phys. Rev. Appl.* **20**, 034005 (2023).
- [12] A. Assouline, L. Pugliese, H. Chakraborti, S. Lee, L. Bernabeu, M. Jo, K. Watanabe, T. Taniguchi, D. C. Glattli, N. Kumada, H. S. Sim, F. D. Parmentier, and P. Roulleau, Emission and coherent control of levitons in graphene, *Science* **382**, 1260 (2023).
- [13] E. Bocquillon, V. Freulon, F. D. Parmentier, J. M. Berroir, B. Placais, C. Wahl, J. Rech, T. Jonckheere, T. Martin, C. Grenier, D. Ferraro, P. Degiovanni, and G. Fève, Electron quantum optics in ballistic chiral conductors, *Annalen Der Physik* **526**, 1 (2014).
- [14] N. Ubbelohde, L. Freise, E. Pavlovska, P. G. Silvestrov, P. Recher, M. Kokainis, G. Barinovs, F. Hohls, T. Weimann, K. Pierz, and V. Kashcheyevs, Two electrons interacting at a mesoscopic beam splitter, *Nature Nanotechnology* **18**, 733 (2023).
- [15] J. D. Fletcher, W. Park, S. Ryu, P. See, J. P. Griffiths, G. A. C. Jones, I. Farrer, D. A. Ritchie, H. S. Sim, and M. Kataoka, Time-resolved coulomb collision of single electrons, *Nature Nanotechnology* **18**, 727 (2023).
- [16] J. Wang, H. Edlbauer, A. Richard, S. Ota, W. Park, J. Shim, A. Ludwig, A. D. Wieck, H. S. Sim, M. Urdampilleta, T. Meunier, T. Kodera, N. H. Kaneko, H. Sellier, X. Waintal, S. Takada, and C. Bauerle, Coulomb-mediated antibunching of an electron pair surfing on sound, *Nature Nanotechnology* **18**, 721 (2023).
- [17] C. Bäuerle, D. C. Glattli, T. Meunier, F. Portier, P. Roche, P. Roulleau, S. Takada, and X. Waintal, Coherent control of single electrons: a review of current progress, *Reports on Progress in Physics* **81**, 056503 (2018).
- [18] H. Edlbauer, J. Wang, T. Crozes, P. Perrier, S. Ouacel, C. Geffroy, G. Georgiou, E. Chatzikyriakou, A. Lacerda-Santos, X. Waintal, D. C. Glattli, P. Roulleau, J. Nath, M. Kataoka, J. Splettstoesser, M. Acciai, M. C. da Silva Figueira, K. Öztas, A. Trelakis, T. Grange, O. M. Yevtushenko, S. Birner, and C. Bäuerle, Semiconductor-based electron flying qubits: review on recent progress accelerated by numerical modelling, *EPJ Quantum Technology* **9**, 21 (2022).
- [19] D. Pomaranski, R. Ito, N. H. Tu, A. Ludwig, A. D. Wieck, S. Takada, N.-H. Kaneko, S. Ouacel, C. Bauerle, and M. Yamamoto, Semiconductor circuits for quantum computing with electronic wave packets (2024), arXiv:2410.16244 [cond-mat.mes-hall].
- [20] S. Ouacel, L. Mazzella, T. Kloss, M. Aluffi, T. Vasselon, H. Edlbauer, J. Wang, C. Geffroy, J. Shaju, M. Yamamoto, D. Pomaranski, S. Takada, N.-H. Kaneko, G. Georgiou, X. Waintal, M. Urdampilleta, A. Ludwig, A. D. Wieck, H. Sellier, and C. Bäuerle, Electronic interferometry with ultrashort plasmonic pulses (2024), arXiv:2408.13025 [cond-mat.mes-hall].
- [21] H. Bartolomei, E. Frigerio, M. Ruelle, G. Reborra, Y. Jin, U. Gennser, A. Cavanna, E. Baudin, J.-M. Berroir, I. Safi, P. Degiovanni, G. C. Ménard, and G. Fève, Time-resolved sensing of electromagnetic fields with single-electron interferometry (2024), arXiv:2408.12903 [cond-mat.mes-hall].
- [22] K. A. Matveev and L. I. Glazman, Coulomb blockade of tunneling into a quasi-one-dimensional wire, *Phys. Rev. Lett.* **70**, 990–993 (1993).
- [23] E. Berg, Y. Oreg, E. A. Kim, and F. von Oppen, Fractional charges on an integer quantum hall edge, *Phys. Rev. Lett.* **102**, 236402 (2009).
- [24] H. Inoue, A. Grivnin, N. Ofek, I. Neder, M. Heiblum, V. Umansky, and D. Mahalu, Charge fractionalization in the integer quantum hall effect, *Phys. Rev. Lett.* **112**, 166801 (2014).
- [25] T. Lorenz, M. Hofmann, M. Gruninger, A. Freimuth, G. S. Uhrig, M. Dumm, and M. Dressel, Evidence for spin-charge separation in quasi-one-dimensional organic conductors, *Nature* **418**, 614 (2002).
- [26] O. M. Auslaender, H. Steinberg, A. Yacoby, Y. Tserkovnyak, B. I. Halperin, K. W. Baldwin, L. N. Pfeiffer, and K. W. West, Spin-charge separation and localization in one dimension, *Science* **308**, 88–92 (2005).

- [27] Y. Jompol, C. J. B. Ford, J. P. Griffiths, I. Farrer, G. A. C. Jones, D. Anderson, D. A. Ritchie, T. W. Silk, and A. J. Schofield, Probing spin-charge separation in a tomonaga-luttinger liquid, *Science* **325**, 597–601 (2009).
- [28] H. Kamata, N. Kumada, M. Hashisaka, K. Muraki, and T. Fujisawa, Fractionalized wave packets from an artificial tomonaga-luttinger liquid, *Nature Nanotechnology* **9**, 177–181 (2014).
- [29] V. Freulon, A. Marguerite, J. M. Berroir, B. Placais, A. Cavanna, Y. Jin, and G. Feve, Hong-ou-mandel experiment for temporal investigation of single-electron fractionalization, *Nature Communications* **6**, 6854 (2015).
- [30] M. Hashisaka, N. Hiyama, T. Akiho, K. Muraki, and T. Fujisawa, Waveform measurement of charge- and spin-density wavepackets in a chiral tomonaga-luttinger liquid, *Nature Physics* **13**, 559–562 (2017).
- [31] M. Yamamoto, S. Takada, C. Bäuerle, K. Watanabe, A. D. Wieck, and S. Tarucha, Electrical control of a solid-state flying qubit, *Nature Nanotechnology* **7**, 247–251 (2012).
- [32] A. V. Chaplik, Absorption and emission of electromagnetic waves by two-dimensional plasmons, *Surface Science Reports* **5**, 289–335 (1985).
- [33] J. Wu, A. S. Mayorov, C. D. Wood, D. Mistry, L. Li, W. Muchenje, M. C. Rosamond, L. Chen, E. H. Linfield, A. G. Davies, and J. E. Cunningham, Excitation, detection, and electrostatic manipulation of terahertz-frequency range plasmons in a two-dimensional electron system, *Scientific Reports* **5**, 15420 (2015).

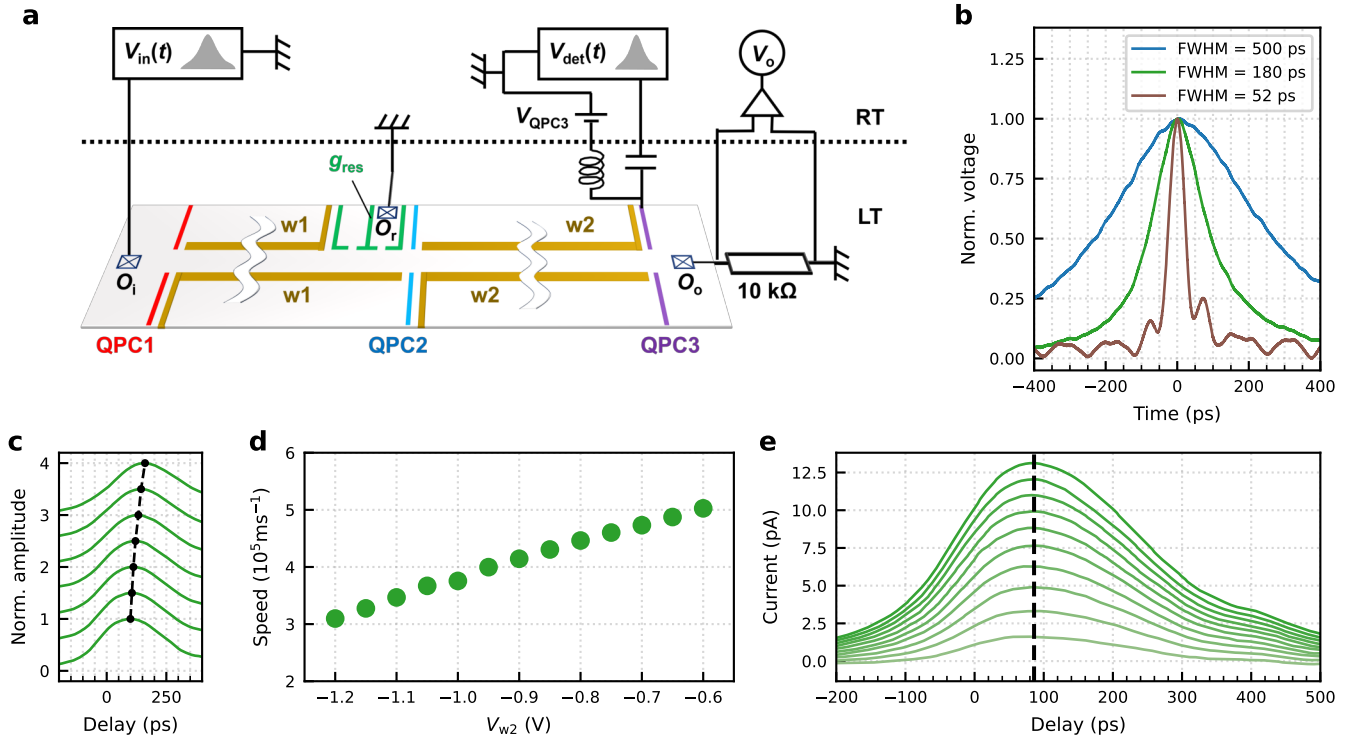


**FIG. 1. Experimental setup and time-resolved measurement of plasmon wavepackets.** **a.** Schematic of the device and the measurement setup. A  $50\text{ }\mu\text{m}$ -long electron waveguide can be formed by polarising gates w2 and its length can be extended to  $100\text{ }\mu\text{m}$  by additionally polarising gates w1, and  $g_{res}$ . QPC1 and QPC2 are used to locally control the number of transmitting electron conduction channels for the  $100\text{ }\mu\text{m}$  and  $50\text{ }\mu\text{m}$  long waveguide, respectively. QPC3 is used for time-resolved measurements of plasmon wavepackets. A high bandwidth bias tee is connected to the upper QPC3 gate to be able to apply a fast voltage pulse,  $V_{det}(t)$  on top of the dc voltage,  $V_{QPC3}$ . The reservoir gate  $g_{res}$  is used to connect the  $100\text{ }\mu\text{m}$ -long electron waveguide to the Ohmic contact,  $O_r$ . Plasmon wavepackets are excited by applying a voltage pulse,  $V_{in}(t)$ , on the Ohmic contact,  $O_i$ . The output current at the Ohmic contact,  $O_o$ , is measured by the voltage,  $V_o$  across a cold  $10\text{ k}\Omega$  resistor. **b.** Temporal shape of the voltage pulses generated by the AWG, with pulse widths ranging from 52 ps to 500 ps. **c.** Time-resolved measurement of plasmon wavepackets excited by a 180 ps-long voltage pulse, for different wire widths in the  $50\text{ }\mu\text{m}$ -long quantum wire. The vertical scale is normalised to one. Each curve is offset vertically for clarity. The gate voltage  $V_{w2}$  is changed from  $-0.6\text{ V}$  at the bottom to  $-1.2\text{ V}$  at the top by  $-0.1\text{ V}$  step. The peak positions are indicated with black points. **d.** Speed of plasmon wavepackets excited by a 180 ps-long voltage pulse as a function of the gate voltage,  $V_{w2}$ . The speed is calculated from the length of the quantum wire and the delay time at the peak obtained as in **c.** **e.** Time-resolved measurements of plasmon wavepackets excited by a 180 ps-long voltage pulse with varying pulse amplitudes. The peak voltage at  $O_i$  is adjusted between 0.24 mV and 2.4 mV. The dashed line highlights the unchanged peak position despite varying pulse amplitudes. These characterisation measurements were conducted at 4 K.

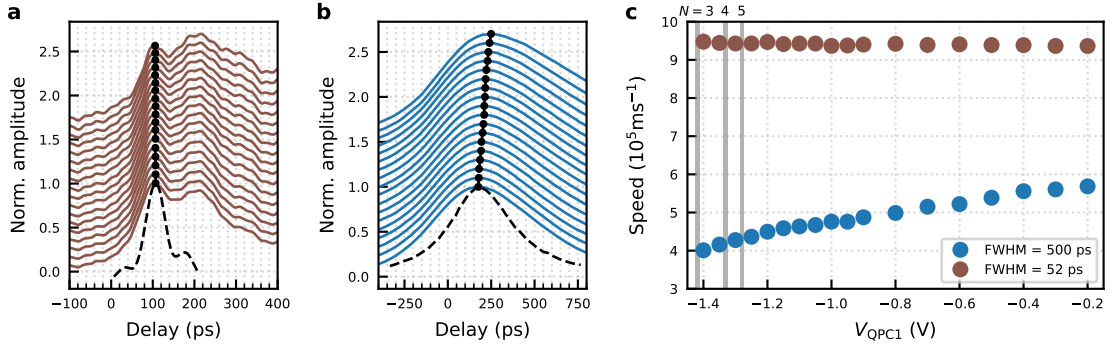


FIG. 2. **Local control of the number of transmitting electron conduction channels in 100  $\mu\text{m}$  quantum wire.** **a, b.** Time-resolved measurement of plasmon wavepackets excited by 52 ps-long voltage pulse (**a**) and 500 ps-long voltage pulse (**b**) for different voltages on the gates of QPC1. The amplitude is normalized to one. Each curve is offset vertically for clarity. The gate voltage  $V_{\text{QPC1}}$  was stepped from  $-0.2\text{ V}$  at the bottom to  $-1.4\text{ V}$  at the top. The peak position is indicated by the black circles. The shape of the voltage pulse used to excite the plasmon wavepacket is drawn by the black dashed line. **c.** Speed of the plasmon wavepackets calculated from the peak delay indicated by the black circles in **a, b**. Here  $N$  indicates the number of transmitting electron channels across QPC1 in each grey shaded gate-voltage range.

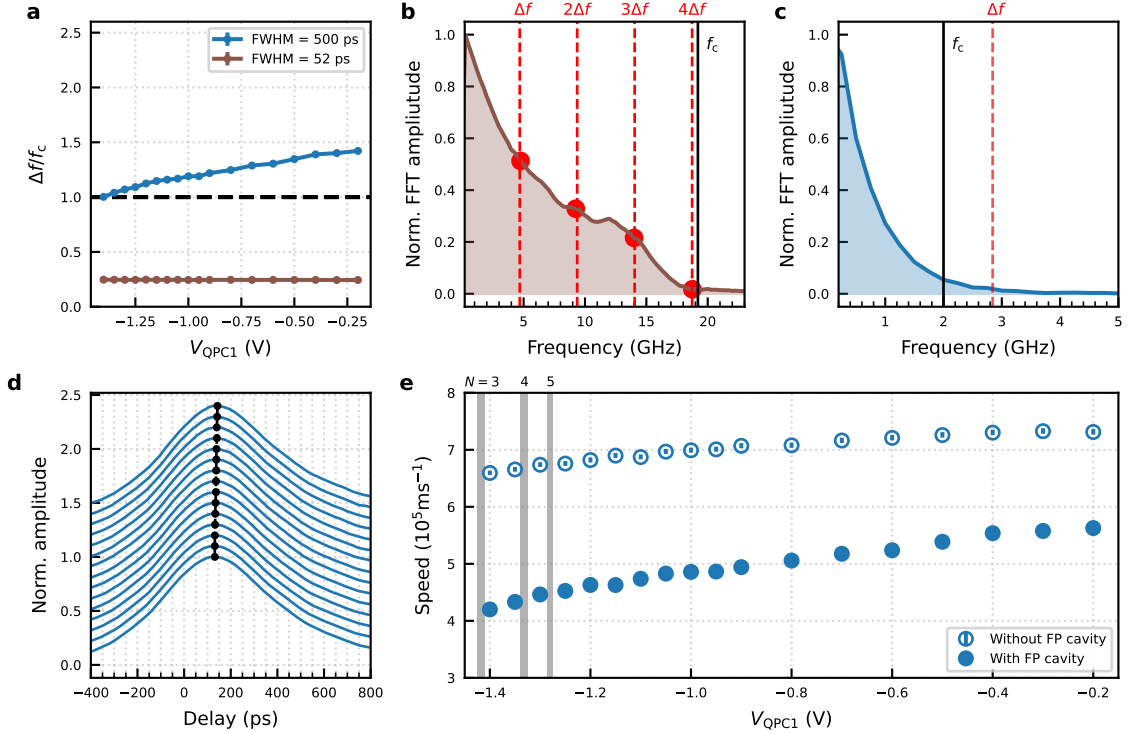


FIG. 3. **Fabry-Pérot cavity and speed control with a local constriction.** **a.** The ratio between the frequency quantisation of the Fabry-Pérot cavity,  $\Delta f$ , and the cut-off frequency,  $f_c$  for the plasmon wavepackets. The dashed line indicates  $\Delta f/f_c = 1$ .  $\Delta f$  ( $= v_p/2L_{\text{FP}}$ ) as a function of  $V_{\text{QPC1}}$  is calculated from  $v_p$  in Fig. 2c.  $f_c$  ( $= 1/t_{\text{FWHM}}$ ) is calculated from  $t_{\text{FWHM}}$  in Fig. 1b. **b, c.** Normalised amplitude of fast Fourier transform (FFT) of the voltage pulse in Fig. 1b for 52 ps-long voltage pulse (**b**) and 500 ps-long voltage pulse (**c**). The cut-off frequency,  $f_c$ , is indicated by a black solid line. In addition,  $\Delta f$  at  $V_{\text{QPC1}} = -0.2\text{ V}$  and its multiples are indicated by the red dashed lines. **d.** Time-resolved measurement of a plasmon wavepacket excited by 500 ps pulse for different gate voltages applied to QPC1 in the 100  $\mu\text{m}$ -long electronic waveguide while it is connected to the Ohmic contact  $O_r$ . The amplitude is normalized to one. Each curve is offset vertically for clarity. The gate voltage  $V_{\text{QPC1}}$  was stepped from  $-0.2\text{ V}$  (bottom) to  $-1.4\text{ V}$  (top). The peak position is indicated by the black dots. **e.** Speed of the plasmon wavepackets with and without the FP cavity (without and with the connection to  $O_r$ ) as a function of  $V_{\text{QPC1}}$ . The data with the FP cavity are the same as in Fig. 2c for the plasmon wavepackets excited by 500 ps-long voltage pulse. Here  $N$  indicates the number of transmitting electron channels across QPC1 in each grey shaded gate-voltage range.

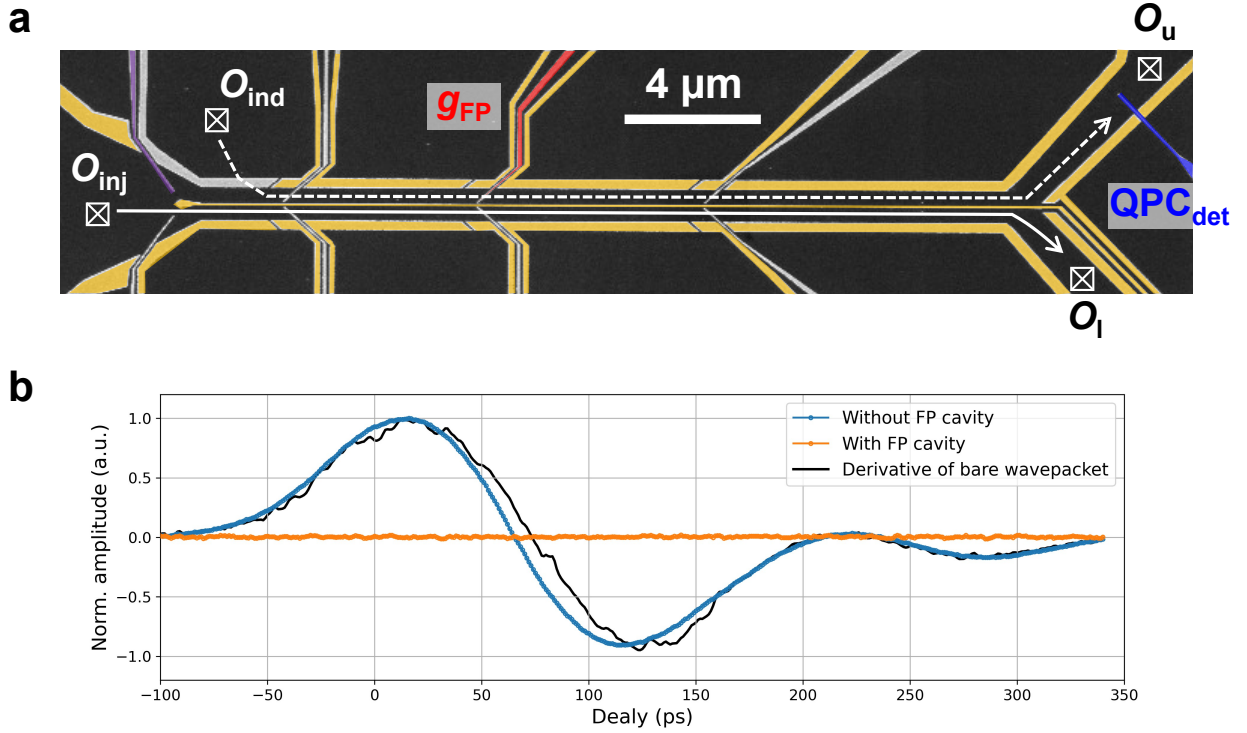


FIG. 4. **Induced plasmon wavepacket in parallel electron waveguides.** **a.** SEM image of the device to investigate induced plasmon wavepackets. The gates coloured in yellow and purple are used to electrostatically form the circuit for the measurement. As a result, two parallel electron waveguides, which are electrically isolated, are defined. Time-resolved measurements of the induced plasmon wavepackets, injected at the Ohmic  $O_{inj}$ , are performed with the gate,  $QPC_{det}$ . A Fabry-Pérot (FP) cavity can be formed by creating a potential barrier with the gate,  $g_{FP}$ , indicated in red. **b.** Induced plasmon wavepacket without (blue curve) and with the FP cavity (orange curve). The amplitude is normalized with the maximum of the data without the FP cavity. The black solid curve is derivative of the bare plasmon wavepacket measured in a slightly different setup (see Fig. S7).

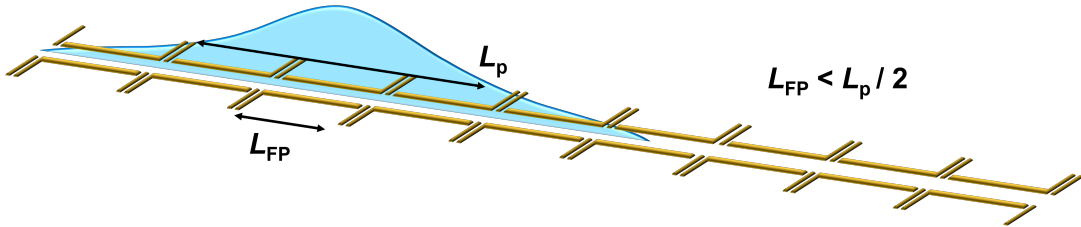


FIG. 5. **Schematic of the proposed device structure realizing a clean and long one-dimensional system.** QPCs are placed at the distance,  $L_{FP}$ , shorter than the half length of the plasmon wavepacket,  $L_p/2$ . When the number of transmitting channels is locally reduced to be one at each QPC, a clean and long one-dimensional system can be realised. Since the width of the quantum wires can be kept wide, the system is less vulnerable to the potential fluctuation of the surrounding environment due to the screening effect with electrons in many conduction channels.

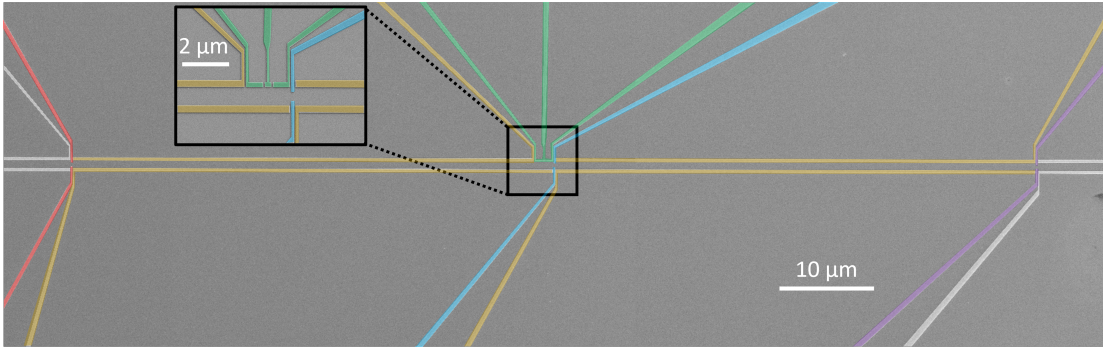


FIG. S1. **Scanning electron micrograph of the device.** False colors are used to indicate the gates used for the experiment and correspond to the ones employed in Fig. 1a. The inset is the focus around QPC2. The gates without the false colors are not used in this experiment.

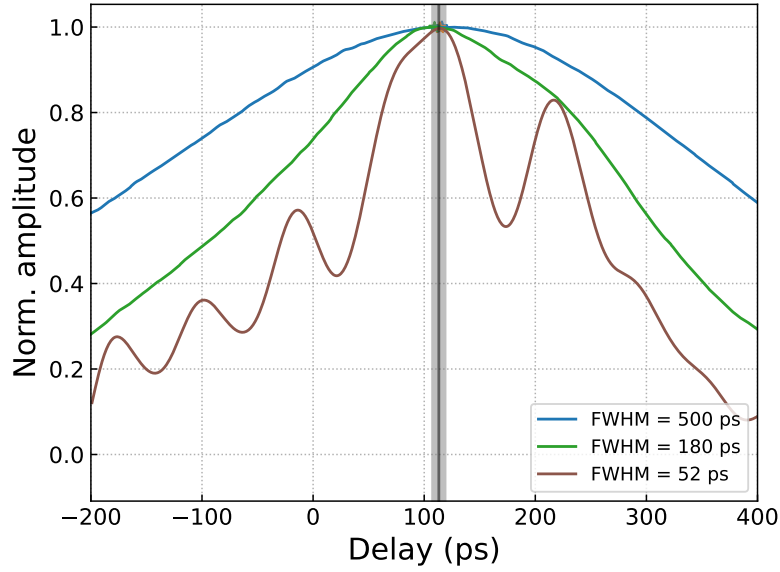


FIG. S2. **Calibration of RF line delay time using a two dimensional plasmon.** A two dimensional plasmon is excited by applying the voltage pulse with different full width at half maximum (FWHM) on the contact,  $O_i$  without applying any voltage on the gates ( $w_1$ ,  $w_2$ , QPC1, QPC2,  $g_{res}$ ). The time-resolved measurement is performed by using QPC3 as explained in the main text. The peak position does not change for different pulse lengths and is estimated to be 111(6) ps.

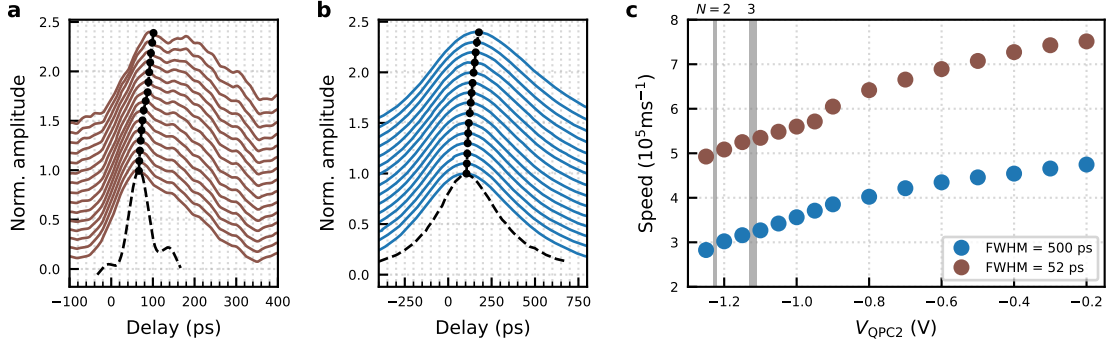


FIG. S3. **Local control of the number of transmitting electron conduction channels in 50  $\mu\text{m}$ -quantum wire.** **a, b.** Time-resolved measurement of plasmon wavepackets excited by 52 ps-long voltage pulse (**a**) and 500 ps-long voltage pulse (**b**) for different voltages on the gates of QPC2. The amplitude is normalized to one. Each curve is offset vertically for clarity. The gate voltage  $V_{\text{QPC2}}$  was stepped from  $-0.2\text{ V}$  at the bottom to  $-1.25\text{ V}$  at the top. The peak position is indicated by the black circles. The shape of the voltage pulse used to excite the plasmon wavepacket is drawn by the black dashed line. **c.** Speed of the plasmon wavepackets calculated from the peak delay indicated by the black circles in **a, b**. Here  $N$  indicates the number of transmitting electron channels across QPC2 in each grey shaded gate-voltage range.

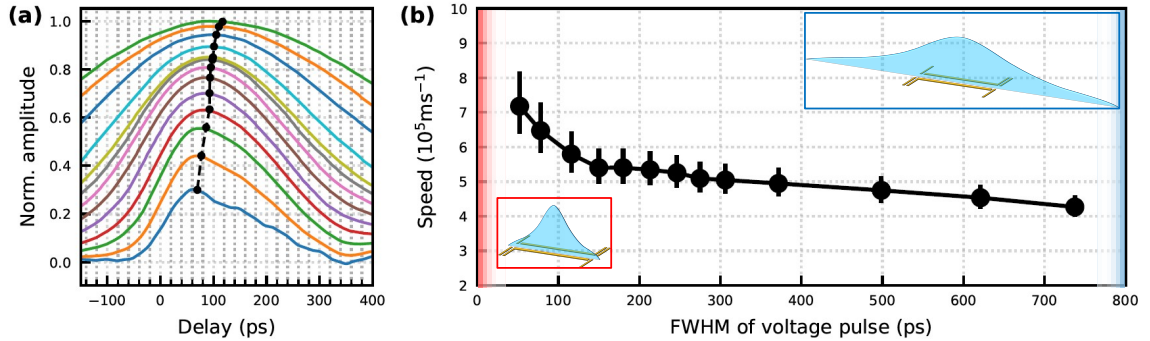


FIG. S4. **Temporal width dependent plasmon speed in 50  $\mu\text{m}$ -quantum wire.** **a.** Time-resolved measurement of plasmon wavepackets excited by the voltage pulse having different FWHM. The FWHM of each pulse is as follows: 52 ps (bottom blue curve), 78 ps, 116 ps, 150 ps, 180 ps, 213 ps, 246 ps, 275 ps, 306 ps, 372 ps, 500 ps, 631 ps, and 737 ps. The peak position detected by Lorentzian curve fitting is indicated by the black points. **b.** Speed of plasmon wavepackets as a function of FWHM of the voltage pulse used for excitation. Schematics inside the figure show the situation where  $L_p \lesssim L$  (red box) and  $L_p > L$  (blue box). For longer plasmon pulses, the plasmon speed gradually decreases, as also shown in Fig. 2. In the adiabatic limit, where the plasmon temporal duration is large and approaches the DC transport limit, the plasmon speed is decreased and converges towards the electron's Fermi velocity in the 2DEG,  $\sim 2.3 \times 10^5\text{ m/s}$ . At this limit, the plasmon velocity does not depend much on the plasmon duration. In contrast, by decreasing the plasmon duration, we observe that the speed is linearly increased. In the non-adiabatic limit, where the plasmon duration is shorter than the quantum wire, we observe a rapid increase of the plasmon speed ( $< 100\text{ ps}$ ). This suggests that the interactions between the electrons becomes important, thus forcing the plasmon to spread into other conduction channels and consequently the speed to be renormalised. In this limit, there is one dominant fast plasmon speed.

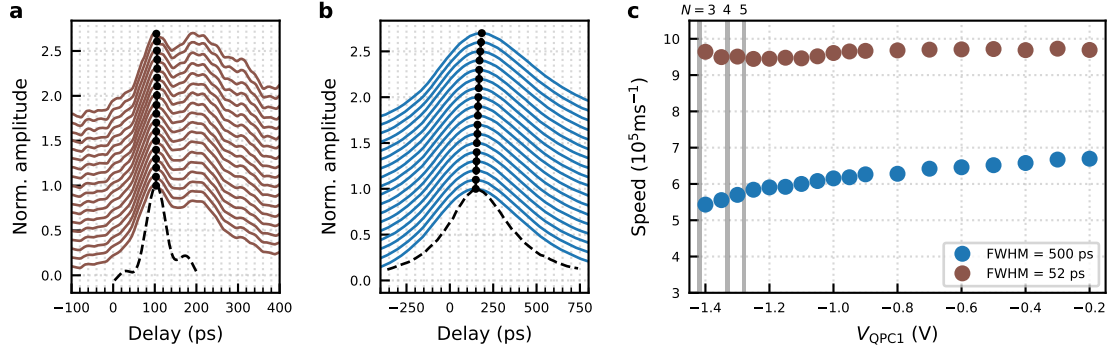


FIG. S5. **Local control of the number of transmitting electron channels in  $100 \mu\text{m}$ -quantum wire at 4 K.** **a, b.** Time-resolved measurement of plasmon wavepackets excited by 52 ps-long voltage pulse (**a**) and 500 ps-long voltage pulse (**b**) for different voltages on the gates of QPC1. The amplitude is normalized to one. Each curve is offset vertically for clarity. The gate voltage  $V_{\text{QPC1}}$  was stepped from  $-0.2 \text{ V}$  at the bottom to  $-1.4 \text{ V}$  at the top. The peak position is indicated by the black circles. The shape of the voltage pulse used to excite the plasmon wavepacket is drawn by the black dashed line. **c.** Speed of the plasmon wavepackets calculated from the peak delay indicated by the black circles in **a, b**. Here  $N$  indicates the number of transmitting electron channels across QPC1 in each grey shaded gate-voltage range. The gate voltage configuration is slightly modified from the same measurement at the base temperature shown in Fig. 2. This results in the slightly different absolute speeds of plasmon wavepackets.

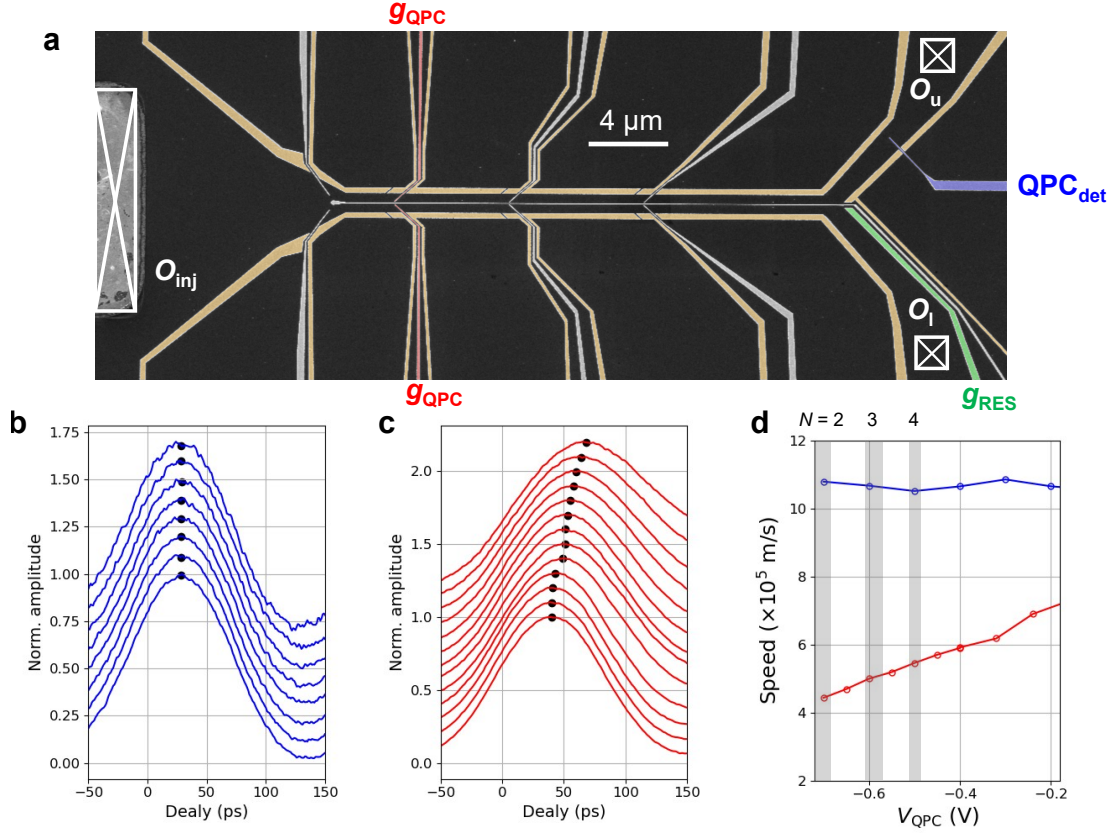


FIG. S6. **Speed measurement as a function of a local constriction in three terminal device.** **a.** The scanning electron micrograph image of the three terminal device. This is the same device as in Fig. 4. For the measurement, the gates without false colour including the narrow middle gate are not polarised. The gates coloured in orange are polarised to form a single electron waveguide. The width of the waveguide is kept wide hosting more than 30 conduction channels. The time-resolved measurement is performed by using the gate  $\text{QPC}_{\text{det}}$ . When a relatively small negative voltage is applied on the gate  $g_{\text{RES}}$ , this device works as a three terminal device. On the other hand, when a large negative voltage is applied on the gate  $g_{\text{RES}}$  to pinch off the connection to the contact,  $O_1$ , the device becomes a two terminal device. In this measurement, we use a Gaussian shaped voltage pulse whose FWHM is about 83 ps for both the excitation of plasmon wavepackets and the time-resolved measurement with  $\text{QPC}_{\text{det}}$ . The peak amplitude of the excitation voltage pulse is  $\sim 0.5$  mV. **b.** Time-resolved measurement of plasmon wavepackets in the three-terminal situation. The different curves are taken at different voltages on the gates  $g_{\text{QPC}}$ . The amplitude is normalized to one and the different curves are offset vertically for clarity. **c.** Time-resolved measurement as **b** in the two-terminal situation. **d.** Speed of plasmon wavepackets as a function of the voltage on  $g_{\text{QPC}}$  for the three-terminal situation (blue) and the two-terminal situation (red). The speed of plasmon wavepackets is modified with  $g_{\text{QPC}}$  only for the two-terminal situation.  $N$  indicates the number of transmitting electron channels across  $g_{\text{QPC}}$  in each grey shaded gate-voltage range.

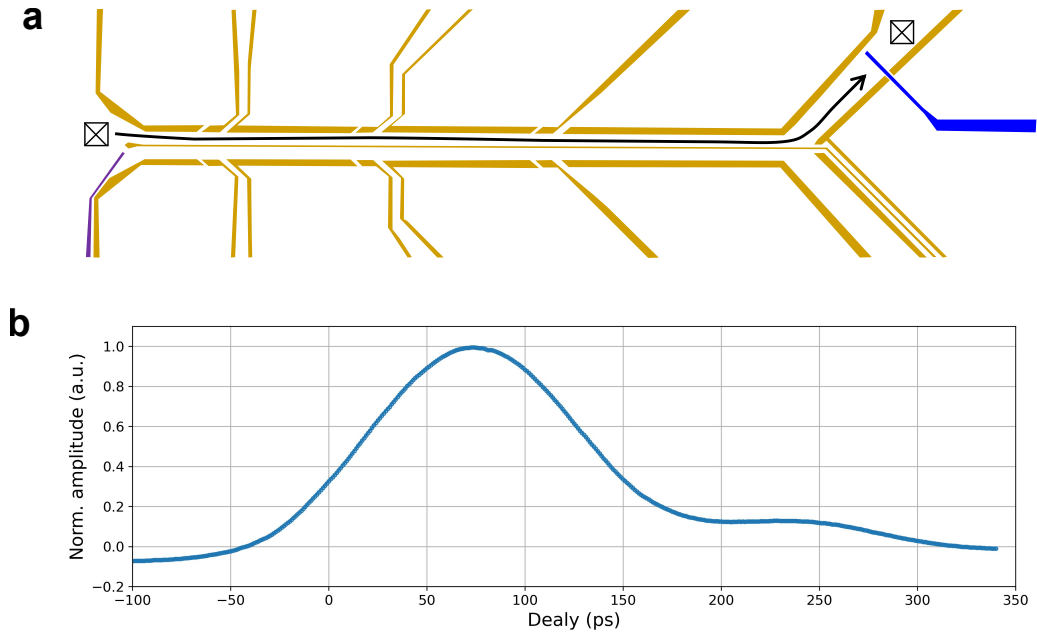


FIG. S7. **Time-resolved measurement of the injected plasmon wavepacket.** **a.** Schematic showing the device configuration to perform time-resolved measurement of the injected plasmon wavepacket. Here plasmon wavepackets are injected to the upper electron waveguide by closing the lower gate at the entrance highlighted in purple. **b.** Time-resolved measurement of the injected plasmon wavepacket. The observed shape is the convolution of the bare wavepacket shape and opening of the detection gate. Both excitation of the plasmon wavepacket and opening of the detection gate are performed with 83 ps-long voltage pulse from AWG (Keysight M8190A).